Journal of Convex Analysis
Volume 32 (2025), No. 2, 487–510

Basin Sensitivity via Continuity of Multiset-Valued Mappings

Adam B. Levy
Department of Mathematics, Bowdoin College, 8600 College Station, Brunswick, Maine, U.S.A.
alevy@bowdoin.edu

Dedicated to Ralph Tyrrell Rockafellar on the occasion of his 90th birthday.

Received: January 2, 2024
Accepted: April 7, 2024

Basins of attraction consist of the initial iterates from which a minimization method applied to an objective function clusters at the same attractor, and we aim to analyze the sensitivity of basins of attraction to perturbations in the objective function. We do this by developing various continuity properties for "multiset-valued mappings" that generalize traditional notions of continuity for mappings. We apply those continuity properties to the particular case of "basin mappings" that map a parameter to the basins of attraction resulting from that perturbation in the objective. We explore our results through simulation and we develop new "grid continuity" properties where sampling is intrinsic. Finally, we connect grid continuity to our generalized versions of more traditional continuity properties.

Keywords: Basin of attraction, numerical minimization, sensitivity analysis, multiset-valued mappings, continuity.

2020 Mathematics Subject Classification: 49J53, 49K40, 65K99, 90C31

1. Introduction

Multisets can contain elements in multiple instances, and an important occurrence of these comes from numerical minimization methods that update "iterate-multisets" at each iteration (e.g., [8]). For instance, the Nelder-Mead method from [13] applied to an objective function of n-variables updates a "simplex" of $n+1$ points from one iteration to the next, and these sets of points typically cluster toward a multiset containing $n+1$ copies of a minimizer when the method is successful.

In this context, a "basin of attraction" was defined in [8] (and expanded in [9] and [10]) to be the collection of initial iterate-mutlisets from which a minimization method clusters toward a particular attractor x^∞ of the method applied to an objective function f. Basins of attraction have been studied in a variety of contexts, including dynamical systems (e.g., [1], [4], [5], [6], [7], [16], [17]), nonlinear equations (e.g., [20], [21], [22]), and numerical optimization (e.g., [2], [3], [11], [12], [14], [18], [19]). In the present paper, we analyze the sensitivity to perturbation of basins of attraction in numerical minimization by developing continuity properties that apply to "basin mappings" associating parameters $\beta \in \mathbb{R}^d$ to the basins of attraction associated with perturbed objective functions $f_\beta : \mathbb{R}^n \to \mathbb{R} \cup \{\infty\}$. Measuring this sensitivity can help us better understand how the performance of a minimization method is affected by inaccuracies in the data of a minimization problem.

ISSN 0944-6532 / $ 2.50

Basin mappings take points $\beta \in \mathbb{R}^d$ to collections of multisets, and we generalize this in Section 2 with the new concept of a "multiset-valued mapping", whose semicontinuity properties we also introduce and explore. In Section 3, we develop concepts of the "**d**-excess" of one collection of multisets over another and the **d**-distance between a pair of collections of multisets, both in terms of a "pre-distance function" **d**. We use these concepts to define **d**-Lipschitz continuity and **d**-calmness properties for multiset-valued mappings, and we investigate these properties through examples to see how basins of attraction might respond to perturbations of the objective function. Some of our investigation is done through simulation by repeatedly running the minimization method from a sample of initial iterate-multisets. Such simulations are naturally restricted to a bounded sampling region, so we extend a traditional form of localized continuity to a concept here of "truncated" continuity that compares only multisets whose elements come from a specified region. Another feature of simulation is that it can only consider a finite number of samples, and, in Section 4, we develop notions of "grid continuity" where finite sampling is intrinsic. We subsequently connect grid continuity to truncated **d**-Lipschitz continuity through our main result, Theorem 4.4, and we finish with a section describing how one might use investigations of grid continuity to pre-process whether a basin mapping might be truncated **d**-Lipschitz continuous.

2. Continuity of multiset-valued mappings

Multisets are collections of elements from a normed vector space where the same elements may appear in multiple instances, and "multiset mappings" were introduced in [8] to describe maps of individual multisets in a domain space to individual multisets in a range space. These objects are a generalization of set-valued mappings (also called multifunctions) that map points to collections of points, and we now generalize both of these types of mappings with a *multiset-valued mapping* that maps multisets from a domain space to collections of multisets in a *range space* $\mathcal{X}$. (A more descriptive, but less compact, label for these objects might be "set-valued multiset mappings".)

For our sensitivity analysis, the simple perturbations $\beta \in \mathbb{R}^d$ of an objective function will be the "multisets" in the domain space (i.e., not actually multisets), so we will focus here entirely on multiset-valued mappings with the domain space $\mathbb{R}^d$ of individual elements β. Our continuity properties for such multiset-valued mappings will be stated in terms of the domain of the multiset-valued mapping

$$\mathrm{dom}\,(M) := \left\{\beta \in \mathbb{R}^d : M(\beta) \neq \emptyset\right\},$$

as well as a "pre-distance function".

Definition 2.1. (Pre-distance function, [8]) A *pre-distance* function **d** operates on pairs of multisets (X, X') from the same normed vector space and has the following two properties:

(i) non-negative on non-empty multisets:

$$\mathbf{d}(X, X') \geq 0 \quad \text{when } X \neq \emptyset \text{ and } X' \neq \emptyset,$$

(ii) equal the usual distance when applied to single vectors x and x':

$$\mathbf{d}(x, x') = \|x - x'\|.$$

We add subscripts to the generic notation $\mathbf{d}$ in order to distinguish one particular pre-distance function from another. For instance, some useful examples for this investigation are

$$\begin{aligned}
\mathbf{d}_{\inf}(X, X') &= \inf_{x\in X} \inf_{x'\in X'} \|x - x'\| \\
\mathbf{d}_{\mathrm{exc}}(X, X') &= \sup_{x\in X} \inf_{x'\in X'} \|x - x'\| \\
\mathbf{d}_{\sup}(X, X') &= \sup_{x\in X} \sup_{x'\in X'} \|x - x'\|.
\end{aligned}$$

The subscript on the pre-distance $\mathbf{d}_{\mathrm{exc}}$ recognizes that this function is known as the "excess" of X over X'.

For any pre-distance function $\mathbf{d}$ and any collection $\mathcal{B}$ of multisets X, the infimum $\inf_{X\in\mathcal{B}} \mathbf{d}\left(X, \bar{X}\right)$ is the $\mathbf{d}$-distance from the collection $\mathcal{B}$ to the multiset $\bar{X}$. The definition of the $\mathbf{d}$-closure of a collection of multisets uses this notion.

Definition 2.2. ($\mathbf{d}$-closure, [10]) The $\mathbf{d}$-*closure* of a collection of multisets $\mathcal{B}$ is the collection of multisets $\bar{X}$ that have zero $\mathbf{d}$-distance to $\mathcal{B}$:

$$\mathbf{d}\text{-cl}\,(\mathcal{B}) := \left\{\bar{X} : \inf_{X\in\mathcal{B}} \mathbf{d}\left(X, \bar{X}\right) = 0\right\}.$$

We say that $\mathcal{B}$ is $\mathbf{d}$-*closed* if $\mathbf{d}\text{-cl}\,(\mathcal{B}) \subseteq \mathcal{B}$. □

Remark 2.3. Whenever the pre-distance function satisfies $\mathbf{d}\,(X, X) = 0$ for all $X \in \mathcal{B}$, the $\mathbf{d}$-closure $\mathbf{d}\text{-cl}\,(\mathcal{B})$ contains $\mathcal{B}$ (e.g., this is always true for $\mathbf{d}_{\inf}$ and $\mathbf{d}_{\mathrm{exc}}$, and is true for $\mathbf{d}_{\sup}$ when every $X \in \mathcal{B}$ consists of m copies of the same element). If $\mathcal{B}$ is $\mathbf{d}$-closed in this case, then it equals its closure: $\mathcal{B} = \mathbf{d}\text{-cl}\,(\mathcal{B})$. □

Our first continuity properties use the following notions of outer and inner limits associated with a multiset-valued mapping M (extending [15, Definition 5.4] for set-valued mappings):

$$\text{(outer limit)} \qquad \mathbf{d}\text{-}\limsup M(\bar{\beta}) := \left\{ Y : \begin{array}{c} \exists\, \beta^\nu \in \mathrm{dom}(M) \text{ with } \beta^\nu \to \bar{\beta} \\ \text{and } \inf\limits_{X^\nu\in M(\beta^\nu)} \mathbf{d}\,(X^\nu, Y) \to 0 \end{array} \right\}$$

$$\text{(inner limit)} \qquad \mathbf{d}\text{-}\liminf M(\bar{\beta}) := \left\{ Y : \begin{array}{c} \inf\limits_{X^\nu\in M(\beta^\nu)} \mathbf{d}\,(X^\nu, Y) \to 0 \text{ for every} \\ \beta^\nu \in \mathrm{dom}(M) \text{ with } \beta^\nu \to \bar{\beta} \end{array} \right\}.$$

We have the relationship

$$\mathbf{d}\text{-}\liminf M(\bar{\beta}) \subseteq \mathbf{d}\text{-cl}\left(M\left(\bar{\beta}\right)\right) \subseteq \mathbf{d}\text{-}\limsup M(\bar{\beta}) \tag{1}$$

whenever $\bar{\beta} \in \mathrm{dom}(M)$ since then the constant sequence $\beta^\nu = \bar{\beta}$ is a possibility. Our notions of "weak" continuity require the opposite inclusions.

Definition 2.4. (Weak semicontinuity and continuity) The multiset-valued mapping M is *weakly outer* $\mathbf{d}$-*semicontinuous* at $\bar{\beta}$ if

$$\mathbf{d}\text{-}\limsup M(\bar{\beta}) \subseteq \mathbf{d}\text{-cl}\left(M\left(\bar{\beta}\right)\right),$$

and is *weakly inner* $\mathbf{d}$-*semicontinuous* at $\bar{\beta}$ if

$$\mathbf{d}\text{-cl}\left(M\left(\bar{\beta}\right)\right) \subseteq \mathbf{d}\text{-}\liminf M\left(\bar{\beta}\right).$$

The mapping M is called *weakly* $\mathbf{d}$-*continuous* at $\bar{\beta}$ if both conditions hold. □

Continuity demands the same inclusions as weak continuity, but with $M(\bar{\beta})$ in place of its $\mathbf{d}$-closure.

Definition 2.5. (Semicontinuity and continuity) The multiset-valued mapping M is *outer* $\mathbf{d}$*-semicontinuous* at $\bar{\beta}$ if

$$\mathbf{d}\text{-}\limsup M(\bar{\beta}) \subseteq M\left(\bar{\beta}\right),$$

and is *inner* $\mathbf{d}$*-semicontinuous* at $\bar{\beta}$ if

$$M\left(\bar{\beta}\right) \subseteq \mathbf{d}\text{-}\liminf M\left(\bar{\beta}\right).$$

It is called $\mathbf{d}$*-continuous* at $\bar{\beta}$ if both conditions hold.

Remark 2.6. Note that the second inclusion in (1) ensures that the collection of multisets $M(\bar{\beta})$ is $\mathbf{d}$-closed whenever the multiset-valued mapping M is outer $\mathbf{d}$-semicontinuous at $\bar{\beta}$. Note too that if M is $\mathbf{d}$-continuous at $\bar{\beta}$, then the inclusions (1) guarantee that it is also weakly $\mathbf{d}$-continuous at $\bar{\beta}$. □

Example 2.7. Consider the point $x^\infty = (0,0)$ and the simple multiset-valued mapping defined for $\beta > 0$ by

$$M(\beta) = \left\{ \begin{array}{cl} \mathbb{B}_1(x^\infty) & \text{for } \beta \in (0,2) \\ x^\infty & \text{for } \beta \geq 2 \end{array} \right\}, \tag{2}$$

where $\mathbb{B}_1(x^\infty)$ denotes the open ball in $\mathbb{R}^2$ of radius 1 about x^∞. Figure 2.1 shows the two output possibilities for $M(\beta)$ in this case, where the red star represents x^∞. Note that the multisets returned by this mapping (2) all have cardinality $m = 1$, so all pre-distance functions reduce to the usual distance in $\mathbb{R}^2$.

(a) $\beta = 1$ (b) $\beta = 2$

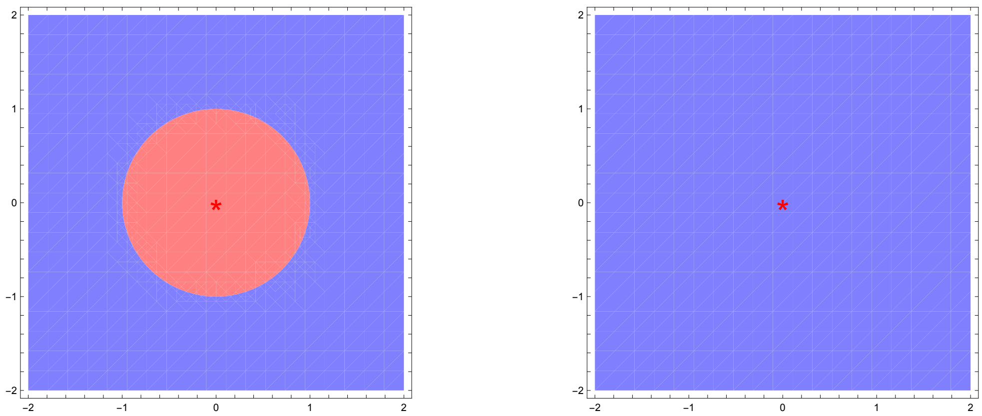

Figure 2.1: Two possibilities for $M(\beta)$ in Example 2.7.

For any $\bar{\beta} \in (0,2)$, the outer and inner limits of the mapping (2) both equal the closed ball $\mathbb{B}_1[x^\infty]$, which is the same as $\mathbf{d}$-cl$\left(M\left(\bar{\beta}\right)\right)$. It follows that this mapping is weakly $\mathbf{d}$-continuous at $\bar{\beta}$. However, since $M(\bar{\beta})$ in this case is the open ball $\mathbb{B}_1(x^\infty)$, this mapping is only inner $\mathbf{d}$-semicontinuous at such $\bar{\beta}$ and not outer $\mathbf{d}$-semicontinuous there.

Moreover, the outer limit $\mathbf{d}$-$\limsup M(2)$ is the closed ball $\mathbb{B}_1[x^\infty]$ and the inner limit is $\mathbf{d}$-$\liminf M(2) = \{x^\infty\}$. Since the $\mathbf{d}$-closure satisfies $\mathbf{d}\text{-cl}\,(M\,(2)) = \{x^\infty\}$, we see that the mapping (2) is *not* weakly $\mathbf{d}$-continuous at $\bar{\beta} = 2$ (it is weakly inner $\mathbf{d}$-semicontinuous there, but not weakly outer $\mathbf{d}$-semicontinuous).

2.1. Basin mappings

Our focus is multiset-valued mappings whose images are "basins of attraction". A minimization method $\mathcal{M}$ applied to an objective function $f : \mathbb{R}^n \to \mathbb{R} \cup \{\infty\}$ defines an *iteration mapping* $I_{\mathcal{M},f}$ operating on *iterate-multisets* $X \subseteq \mathbb{R}^n$ with the same fixed number of elements $|X| = m \geq 1$. When $|X| = 1$, we simply refer to the iterate-multisets as *iterates* and denote them in lowercase x. We also will use the notation $\operatorname{dom}(I_{\mathcal{M},f})$ to denote the collection of iterate-multisets $X \subseteq \mathbb{R}^n$ at which the iteration mapping is nonempty:

$$\operatorname{dom}(I_{\mathcal{M},f}) := \{X : I_{\mathcal{M},f}\,(X) \neq \emptyset\}.$$

In what follows, we use the notation from [15]

$$\mathcal{N}_\infty^{\#} := \{N \subseteq \mathbb{N} : N \text{ infinite}\}$$

to denote the infinite subsets of $\mathbb{N} = \{0, 1, 2, 3, \ldots\}$ and the notation

$$\mathcal{N}_\infty := \{N \subseteq \mathbb{N} : \mathbb{N} \setminus N \text{ finite}\}$$

for the subsequences of $\mathbb{N}$ that include all sufficiently large natural numbers, and we use the notation $\mathbb{N}^+ := \{1, 2, 3, \ldots\}$ for the positive natural numbers. We will also use notion of the *outer limit* of a sequence $\{X^k\}$ of multisets (from [8], extending [15, Definition 4.1]):

$$\limsup_{k\to\infty} X^k := \left\{x^\infty : \exists N \in \mathcal{N}_\infty^{\#},\, \exists x^k \in X^k\ (k \in N) \text{ with } x^k \overset{N}{\to} x^\infty\right\} \tag{3}$$

and the *inner limit* of the same sequence, defined as

$$\liminf_{k\to\infty} X^k := \left\{x^\infty : \exists N \in \mathcal{N}_\infty,\, \exists x^k \in X^k\ (k \in N) \text{ with } x^k \overset{N}{\to} x^\infty\right\}. \tag{4}$$

Definition 2.8. (Attractor, [8]) An *attractor* x^∞ for the iteration mapping $I_{\mathcal{M},f}$ is any element satisfying

$$x^\infty \in \limsup_{k\to\infty} \operatorname{argmin}_f \left(I_{\mathcal{M},f}^{(k)}(X)\right) \text{ for some initial iterate-multiset } X,$$

where $I_{\mathcal{M},f}^{(k)}$ is shorthand for k compositions of the iteration mapping

$$I_{\mathcal{M},f}^{(k)}(X) := \underbrace{I_{\mathcal{M},f} \circ I_{\mathcal{M},f} \circ \ldots \circ I_{\mathcal{M},f}}_{k \text{ times}}(X),$$

and argmin_f is the set of lowest f-valued elements. When the minimization method $\mathcal{M}$ generates iterates x^k, then the f-minimizing argument argmin_f simply returns x^k. However, when $\mathcal{M}$ generates iterate-multisets X^k containing more than one element $|X^k| = m \geq 2$, then the f-minimizing argument argmin_f chooses the lowest f-valued member of each X^k for consideration in the outer limit. □

We also use the stronger concept of attractor that requires convergence for all indices, and not just for an infinite index set N required by the outer limit.

Definition 2.9. (Strong attractor, [10]) The element x^∞ is a *strong attractor* for the iteration mapping $I_{\mathcal{M},f}$ if

$$x^\infty \in \liminf_{k\to\infty} \operatorname{argmin}_f\big(I^{(k)}_{\mathcal{M},f}(X)\big) \text{ for some initial iterate-multiset } X. \qquad \square$$

Remark 2.10. Note that any strong attractor is automatically an attractor since $\mathcal{N}_\infty \subseteq \mathcal{N}^\#_\infty$. $\square$

Definition 2.11. (Basin of attraction, [8]) The *basin of attraction* associated with an attractor x^∞ for $I_{\mathcal{M},f}$ is the collection $\text{Basin}_{\mathcal{M},f}(x^\infty)$ of all attracted initial iterate-multisets:

$$\text{Basin}_{\mathcal{M},f}(x^\infty) := \left\{ X : \begin{array}{l} \exists\, N \in \mathcal{N}^\#_\infty \text{ with } x^k \in \operatorname{argmin}_f\big(I^{(k)}_{\mathcal{M},f}(X)\big) \\ \text{for } k \in N \text{ and } x^k \xrightarrow{N} x^\infty \end{array} \right\}. \qquad \square$$

Definition 2.12. (Strong basin of attraction, [10]) The *strong basin of attraction* associated with a strong attractor x^∞ for $I_{\mathcal{M},f}$ is the collection $\text{S-Basin}_{\mathcal{M},f}(x^\infty)$ of all strongly attracted initial iterate-multisets:

$$\text{S-Basin}_{\mathcal{M},f}(x^\infty) := \left\{ X : \begin{array}{l} \exists\, N \in \mathcal{N}_\infty \text{ with } x^k \in \operatorname{argmin}_f\big(I^{(k)}_{\mathcal{M},f}(X)\big) \\ \text{for } k \in N \text{ and } x^k \xrightarrow{N} x^\infty \end{array} \right\}. \qquad \square$$

We will also use the related notion of an ϵ-basin of attraction from [9] that relies on the following object.

Definition 2.13. (Stepcount function, [9]) Given an attractor x^∞ for $I_{\mathcal{M},f}$, we define the *stepcount function* applied to any iterate-multiset X and any $\epsilon > 0$ by

$$\text{steps}_{x^\infty}(X,\epsilon) := \min\left\{ k \in \mathbb{N} : d_{I^{(k)}_{\mathcal{M},f}(X)}(x^\infty) \le \epsilon \right\}, \tag{5}$$

where

$$d_{I^{(k)}_{\mathcal{M},f}(X)}(x^\infty) := \min_{y \in I^{(k)}_{\mathcal{M},f}(X)} \|y - x^\infty\|$$

is the distance between the iterate-multiset $I^{(k)}_{\mathcal{M},f}(X)$ and the attractor.

Definition 2.14. (ϵ-Basin of attraction, [9]) Given an $\epsilon > 0$, we define the *ϵ-basin of attraction* associated with an attractor x^∞ for $I_{\mathcal{M},f}$ to be the collection of all multisets whose stepcount for that ϵ is finite:

$$\epsilon\text{-Basin}_{\mathcal{M},f}(x^\infty) := \{X : \text{steps}_{x^\infty}(X,\epsilon) < \infty\}.$$

Remark 2.15. From [9, Proposition 1] it follows that an ϵ-basin of attraction always contains the basin of attraction associated with an attractor x^∞:

$$\text{Basin}_{\mathcal{M},f}(x^\infty) \subseteq \epsilon\text{-Basin}_{\mathcal{M},f}(x^\infty) \text{ for any } \epsilon > 0. \qquad \square \tag{6}$$

From a minimization method $\mathcal{M}$, a family of objective functions $f_\beta : \mathbb{R}^n \to \mathbb{R} \cup \{\infty\}$ parameterized by $\beta \in \mathbb{R}^d$, and corresponding attractors x^∞_β, we get the following multiset-valued *basin mappings*:

$$M(\beta) = \text{Basin}_{\mathcal{M},f_\beta}\left(x^\infty_\beta\right),\ M(\beta) = \text{S-Basin}_{\mathcal{M},f_\beta}\left(x^\infty_\beta\right),\ M(\beta) = \epsilon\text{-Basin}_{\mathcal{M},f_\beta}\left(x^\infty_\beta\right),$$

whose images are collections of multisets X in the same finite-dimensional range space $\mathcal{X} = \mathbb{R}^n$, and having the same cardinality $|X| = m \ge 1$.

We illustrate these concepts (and others forthcoming) via examples pairing objective functions on $\mathbb{R}^2$ and minimization methods $\mathcal{M}$ that update iterates, since this combination allows us to readily illustrate the associated basins.

Example 2.16. Consider the family of objective functions

$$f_\beta(x_1, x_2) = \beta\left(\frac{x_1^2 + x_2^2}{2} - \frac{(x_1^2 + x_2^2)^2}{4}\right)$$

parameterized by $\beta \in \mathbb{R}$. For any $\beta > 0$, there is a local minimizer at $x^\infty = (0, 0)$ and a ring of maximizers on the unit circle $x_1^2 + x_2^2 = 1$.

If we apply the steepest-descent method without any line-search, $\mathcal{M} = \mathrm{SD}$, we get the iteration mapping

$$I_{\mathrm{SD}, f_\beta}(x) := x - \nabla f_\beta(x) = x + \beta\left(x_1^2 + x_2^2 - 1\right) x. \tag{7}$$

For any $\beta > 0$, the basins of attraction and strong basins of attraction coincide for the attractor $x^\infty = (0, 0)$:

$$\mathrm{Basin}_{\mathcal{M}, f_\beta}(x^\infty) = \text{S-Basin}_{\mathcal{M}, f_\beta}(x^\infty),$$

and the associated basin mapping $M(\beta) = \mathrm{Basin}_{\mathcal{M}, f_\beta}(x^\infty)$ is given by (2). Figure 2.2 shows the two output possibilities for $M(\beta)$, as generated by pseudo-randomly seeding the iteration mapping and then color-coding each initial point red if the subsequent iterates were attracted to the local minimizer $x^\infty = (0, 0)$ and blue otherwise. (Note that these represent the same two output possibilities pictured in the more traditional plots of Figure 2.)

(a) $\beta = 1$ (b) $\beta = 2$

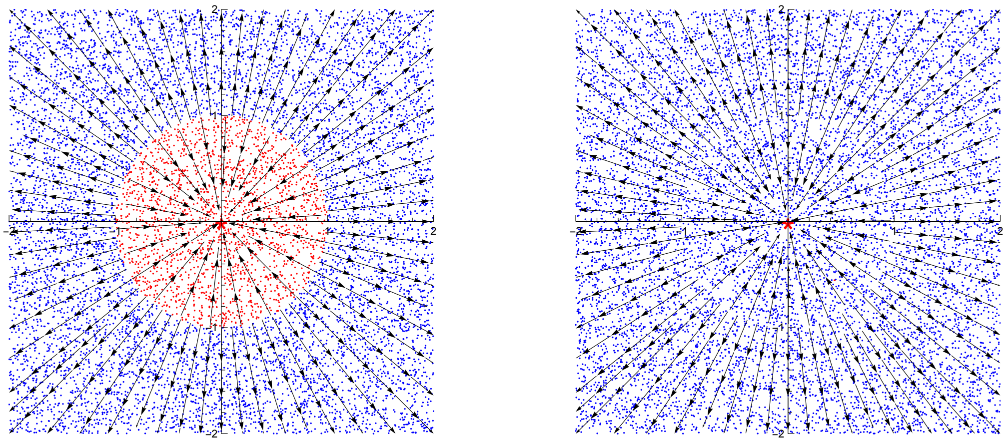

Figure 2.2: The two possibilities for $M(\beta)$ in Example 2.16.

Example 2.17. Consider the family of objective functions f_β from [10, Example 4.3] parameterized by $\beta \in \mathbb{R}$ and defined by

$$f_\beta(x_1, x_2) = \left(x_1^2 + (x_2 + 1)^2\right)\left(x_1^2 + (x_2 - 1)^2 + \beta\right)$$

which have a global minimizer at $x^\infty = (0, -1)$ for any $\beta \geq 0$.

For $\beta \in \left[0, \frac{1}{2}\right)$, the objective f_β also has a local minimizer at

$$x^\infty_\beta = \left(0, \frac{1}{2}(1 + \sqrt{1 - 2\,\beta})\right)$$

and a saddle at $\left(0, \frac{1}{2}\left(1 - \sqrt{1 - 2\,\beta}\right)\right)$. For $\beta = \frac{1}{2}$, the local minimizer and saddle merge (into a saddle). For $-4 < \beta < 0$ the two minimizers switch roles (so, x^∞ is a local minimizer and x^∞_β is a global minimizer), and for $\beta \leq -4$ there is only a single (global) minimizer at x^∞_β and a saddle at $\left(0, \frac{1}{2}\left(1 - \sqrt{1 - 2\,\beta}\right)\right)$.

If we apply the steepest-descent method with Armijo-Goldstein backtracking $\mathcal{M} = \mathrm{AG}$, we get the iteration mapping

$$I_{\mathrm{AG}, f_\beta}(x) := x - \alpha(x)\, \nabla f_\beta(x) \tag{8}$$

in terms of the the step-size function

$$\alpha(x) := \max\Big(\operatorname*{argmax}_{\alpha \in \{2^{-j} : j \in \mathbb{N}\}} \delta_{[0,\infty)} \left(f_\beta(x) - f_\beta\left(x - \alpha\, \nabla f_\beta(x)\right) - \frac{\alpha}{2} \|\nabla f_\beta(x)\|^2 \right) \Big).$$

(a) $\beta = -1.5$ (b) $\beta = -0.5$

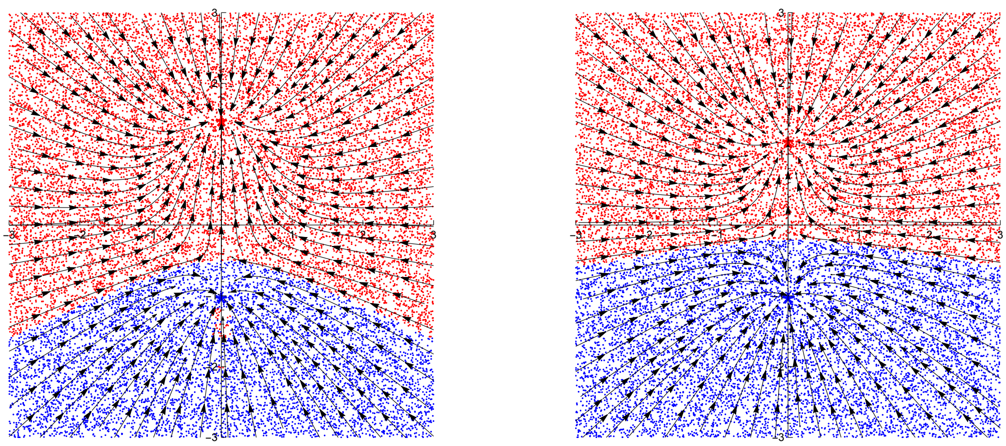

Figure 2.3: The red “island” near $(0, -1)$ disappears, as β increases from -1.5 to -0.5.

Note that the indicator function $\delta_{[0,\infty)}(\cdot)$ for the nonnegative real numbers ensures that this step-size function returns the largest step-size $\alpha = 2^{-j}$ for which the Armijo–Goldstein condition

$$f_\beta(x) - f_\beta\left(x - \alpha\, \nabla f_\beta(x)\right) - \frac{\alpha}{2} \|\nabla f_\beta(x)\|^2 \geq 0$$

is satisfied. Figure 2.3 shows plots of simulated ϵ-basins of attraction for I_{AG, f_β} (with $\epsilon = 0.0001$) where the red basin

$$M(-1.5) = \epsilon\text{-Basin}_{\mathrm{AG}, f_{-1.5}}\left(x^\infty_{-1.5}\right)$$

in Figure 2.1a includes a red “island” of points near the blue attractor $x^\infty = (0, -1)$, that does not appear in the red basin $M(-0.5) = \epsilon\text{-Basin}_{\mathrm{AG}, f_{-0.5}}\left(x^\infty_{-0.5}\right)$ shown in Figure 2.1b.

Figure 2.4 below shows a close-up view of this shrinking red island about the point $\approx (0, -1.225)$ as β increases from -0.7 to -0.5.

$\beta = -0.7$ $\beta = -0.6$ $\beta = -0.5$

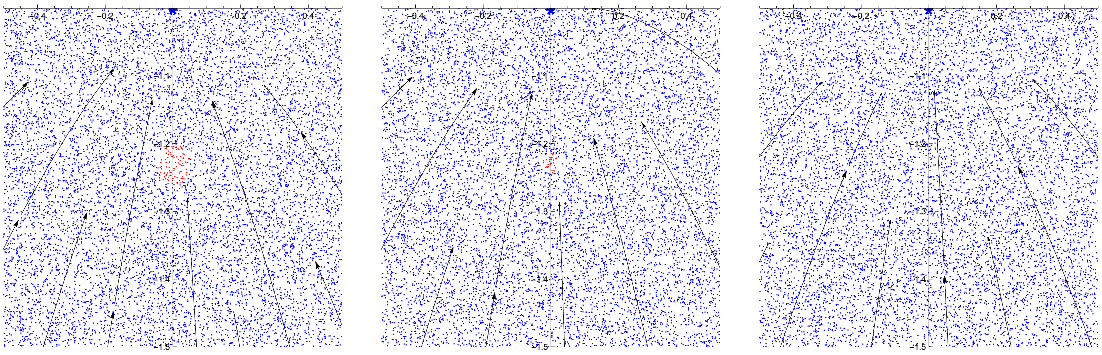

Figure 2.4: Close-up view of disappearing red island near $(0, -1)$.

These simulations suggest that the outer limit $\mathbf{d}\text{-}\limsup M(-0.5)$ of the multiset-valued mapping

$$M(\beta) = \epsilon\text{-Basin}_{\mathrm{AG}, f_\beta}\left(x_\beta^\infty\right) \tag{9}$$

at $\bar{\beta} = -0.5$ would contain the point $(0, -1.225)$, which evidently is not in the collection of multisets $M(-0.5)$ or its $\mathbf{d}$-closure. It follows that M is neither weakly outer $\mathbf{d}$-semicontinuous at $\bar{\beta} = -0.5$ nor $\mathbf{d}$-outer semincontinuous at $\bar{\beta} = -0.5$.

On the other hand, this multiset-valued mapping (9) appears to be at least weakly inner $\mathbf{d}$-semicontinuous at $\bar{\beta} = -0.5$ since only a red region like the one in Figure 2.1b appears in the simulations for $\beta \geq -0.5$ (with no red island about the point $(0, -1.225)$), so that the inner limit $\mathbf{d}\text{-}\liminf M(-0.5)$ looks like the red region in Figure 2.1b.

Finally, the multiset-valued mapping

$$M(\beta) = \epsilon\text{-Basin}_{\mathrm{AG}, f_\beta}\left((0, -1)\right) \tag{10}$$

appears to be at least weakly continuous at $\bar{\beta} = -0.5$ since both the inner limit $\mathbf{d}\text{-}\liminf(-0.5)$ and the outer limit $\mathbf{d}\text{-}\limsup M(-0.5)$ look like the blue region in Figure 2.1b. $\square$

Simulations like those illustrated in Figures 2.3 and 2.4 evidently only cover a bounded sample region of the range space $\mathcal{X}$, so any conclusions drawn are qualified by this limited view of the range space. We extend our continuity properties in the next section by allowing "truncated" versions of multiset-valued mappings.

2.2. Truncated continuity

In this section, we adapt our multiset-valued mapping M by restricting its images to a region Ω of the range space $\mathcal{X}$. The result is the following truncated multiset-valued mapping:

$$M_{\cap\Omega}(\beta) := M(\beta) \cap \Omega,$$

where the intersection here means that *all* elements of a multiset $X \in M(\beta)$ must be in Ω in order to satisfy $X \in M_{\cap\Omega}(\beta)$. The terminology of "truncation" (and notation $M_{\cap\Omega}$) comes from [15] where this was defined for set-valued mappings.

This leads directly to the following notions of truncated continuity.

Definition 2.18. (Truncated weak / strong semicontinuity and continuity)
The multiset-valued mapping M is Ω-*truncated weakly outer* $\mathbf{d}$-*semicontinuous* at $\bar{\beta}$ if the truncated multiset-valued mapping $M_{\cap\Omega}$ is weakly outer $\mathbf{d}$-semicontinuous at $\bar{\beta}$, and M is Ω-*truncated weakly inner* $\mathbf{d}$-*semicontinuous* at $\bar{\beta}$ if $M_{\cap\Omega}$ is weakly inner $\mathbf{d}$-semicontinuous at $\bar{\beta}$. M is called Ω-*truncated weakly* $\mathbf{d}$-*continuous* at $\bar{\beta}$ if both conditions hold.

We say that M is Ω-*truncated outer* $\mathbf{d}$-*semicontinuous* at $\bar{\beta}$ if $M_{\cap\Omega}$ is outer $\mathbf{d}$-semicontinuous at $\bar{\beta}$, and M is Ω-*truncated inner* $\mathbf{d}$-*semicontinuous* at $\bar{\beta}$ if $M_{\cap\Omega}$ is inner $\mathbf{d}$-semicontinuous at $\bar{\beta}$. M is called Ω-*truncated* $\mathbf{d}$-*continuous* at $\bar{\beta}$ if both conditions hold. $\square$

Note that we recover the original "untruncated" concepts simply by setting the region Ω equal to entire range space $\mathcal{X}$.

3. d-Lipschitz continuity of multiset-valued mappings

Our notion of Lipschitz continuity for multiset-valued mappings uses the following concept of the excess of one collection of multisets over another.

Definition 3.1. ($\mathbf{d}$-Excess) For any pre-distance function $\mathbf{d}$ and any pair of collections of multisets $\mathcal{B}$ and $\mathcal{B}'$, we define the $\mathbf{d}$-*excess* of $\mathcal{B}$ over $\mathcal{B}'$ by

$$\mathbf{exc_d}\left(\mathcal{B},\mathcal{B}'\right) := \sup_{X\in\mathcal{B}} \inf_{X'\in\mathcal{B}'} \mathbf{d}\left(X',X\right). \qquad \square$$

Remark 3.2. The $\mathbf{d}$-excess essentially measures the extent to which the second collection fails to overlap the first. For instance, the collections $\mathcal{B} := \{1,2,3\}$ and $\mathcal{B}' := \{1,2\}$ satisfy $\mathbf{exc_d}\left(\mathcal{B},\mathcal{B}'\right) = 1$ for any pre-distance function. This calculation recognizes that the element $3 \in \mathcal{B}$ is 1 unit from its closest point in $\mathcal{B}'$. On the other hand, these same two collections compared in the opposite direction satisfy $\mathbf{exc_d}\left(\mathcal{B}',\mathcal{B}\right) = 0$ since every element in $\mathcal{B}'$ is also contained in $\mathcal{B}$. $\square$

We will want to limit failure to overlap in both directions, so we use both directions in our definition of the "$\mathbf{d}$-distance" between two collections of multisets, which is an extension of the Pompeiu–Hausdorff distance between sets (e.g., [15, Example 4.3]).

Definition 3.3. ($\mathbf{d}$-Distance) For any pre-distance function $\mathbf{d}$ and any pair of collections of multisets $\mathcal{B}$ and $\mathcal{B}'$, we define the $\mathbf{d}$-*distance* between $\mathcal{B}$ and $\mathcal{B}'$ by

$$\mathbf{dist_d}\left(\mathcal{B},\mathcal{B}'\right) := \max\left\{\mathbf{exc_d}\left(\mathcal{B},\mathcal{B}'\right), \mathbf{exc_d}\left(\mathcal{B}',\mathcal{B}\right)\right\}. \qquad \square$$

Remark 3.4. (a) Unlike the $\mathbf{d}$-excess function, the $\mathbf{d}$-distance function is symmetric. (b) One issue with the Pompeiu–Hausdorff distance between sets identified in [15] is that it can be infinite unless the sets are bounded, and our extension to the $\mathbf{d}$-distance between collections of multisets inherits this property. However, the $\mathbf{d}$-distance is guaranteed to be finite whenever the collections consist of multisets whose elements are all contained in some bounded set, and this is a condition we can ensure by truncation. $\square$

When the multisets in two collections are $\mathbf{d}$-closed, then the $\mathbf{d}$-distance is also positive-definite.

Lemma 3.5. (Positive-definite $\mathbf{d}$-distance) *For any collections $\mathcal{B} \neq \emptyset$ and $\mathcal{B}' \neq \emptyset$ of multisets, the $\mathbf{d}$-distance function satisfies*

$$\mathbf{dist_d}\,(\mathcal{B},\mathcal{B}') = 0 \quad \iff \quad \mathcal{B} \subseteq \mathbf{d}\text{-}cl\,\mathcal{B}' \text{ and } \mathcal{B}' \subseteq \mathbf{d}\text{-}cl\,\mathcal{B}. \tag{11}$$

When the collections are $\mathbf{d}$-closed, this implies positive-definiteness:

$$\mathbf{dist_d}\,(\mathcal{B},\mathcal{B}') = 0 \quad \iff \quad \mathcal{B} = \mathcal{B}'.$$

Proof. Recall that

$$\mathbf{dist_d}\,(\mathcal{B},\mathcal{B}') := \max\left\{\sup_{X\in\mathcal{B}}\inf_{X'\in\mathcal{B}'}\mathbf{d}(X',X),\ \sup_{X'\in\mathcal{B}'}\inf_{X\in\mathcal{B}}\mathbf{d}(X,X')\right\}. \tag{12}$$

($\Rightarrow$): If $\mathbf{dist_d}\,(\mathcal{B},\mathcal{B}') = 0$, it follows from the first term in the max on the right side of (12) that for every $X \in \mathcal{B}$, we have $\inf\limits_{X'\in\mathcal{B}'}\mathbf{d}(X',X) = 0$, which means $X \in \mathbf{d}$-cl $\mathcal{B}'$. Similarly from the second term in the max on the right side of (12), we have for every $X' \in \mathcal{B}'$ that $\inf\limits_{X\in\mathcal{B}}\mathbf{d}(X,X') = 0$, which means $X' \in \mathbf{d}$-cl $\mathcal{B}$.

($\Leftarrow$): If $\mathcal{B} \subseteq \mathbf{d}$-cl $\mathcal{B}'$ we know that $\inf\limits_{X'\in\mathcal{B}'}\mathbf{d}(X',X) = 0$ for every $X \in \mathcal{B}$ so that $\sup\limits_{X\in\mathcal{B}}\inf\limits_{X'\in\mathcal{B}'}\mathbf{d}(X',X) = 0$. If $\mathcal{B}' \subseteq \mathbf{d}$-cl $\mathcal{B}$ we know that $\inf\limits_{X\in\mathcal{B}}\mathbf{d}(X,X') = 0$ for every $X' \in \mathcal{B}'$ so that $\sup\limits_{X'\in\mathcal{B}'}\inf\limits_{X\in\mathcal{B}}\mathbf{d}(X,X') = 0$. It follows that $\mathbf{dist_d}\,(\mathcal{B},\mathcal{B}') = 0$ when both of these containments hold as on the right side of (11).

The final statement about positive-definiteness follows immediately from the characterization (11) since $\mathbf{d}$-closedness ensures $\mathbf{d}$-cl $\mathcal{B} = \mathcal{B}$ and $\mathbf{d}$-cl $\mathcal{B}' = \mathcal{B}'$. □

Remark 3.6. Notice that when we substitute $\mathcal{B} = \mathcal{B}'$ in the characterization (11) it gives

$$\mathbf{dist_d}\,(\mathcal{B},\mathcal{B}) = 0 \quad \iff \quad \mathcal{B} = \mathbf{d}\text{-cl}\,\mathcal{B} \qquad \big(\Rightarrow \quad \mathcal{B} \text{ is } \mathbf{d}\text{-closed}\big).$$ □

The following definition of $\mathbf{d}$-Lipschitz continuity uses the notation $\mathbb{B}^d_\delta[\bar\beta]$ to denote the closed ball in $\mathbb{R}^d$ of radius δ about the point $\bar\beta \in \mathbb{R}^d$.

Definition 3.7. ($\mathbf{d}$-Lipschitz continuous) For any pre-distance function $\mathbf{d}$, we say the multiset-valued mapping M is $\mathbf{d}$-*Lipschitz continuous near* $\bar\beta$ if there exists a *radius* $\delta > 0$ and a *modulus* $L > 0$ such that

$$\mathbf{dist_d}\,(M(\beta), M(\beta')) \leq L\,\|\beta - \beta'\| \text{ for all } \beta,\, \beta' \in \mathbb{B}^d_\delta[\bar\beta] \cap \mathrm{dom}(M). \tag{13}$$

Given a region $\Omega \subseteq \mathcal{X}$, we say that M is Ω-*truncated* $\mathbf{d}$-*Lipschitz continuous near* $\bar\beta$ if the truncated multiset-valued mapping $M_{\cap\Omega}(\beta) := M(\beta) \cap \Omega$ is $\mathbf{d}$-Lipschitz continuous near $\bar\beta$. □

Remark 3.8. Note that $\mathbf{d}$-Lipschitz continuity requires in particular that we have $\mathbf{dist_d}\,(M(\beta), M(\beta)) = 0$ for all $\beta \in \mathbb{B}^d_\delta[\bar\beta] \cap \mathrm{dom}(M)$.

Example 3.9. The basin mapping (2) from Examples 2.7 and 2.16 is $\mathbf{d}$-Lipschitz continuous near $\bar\beta = 1$ with radius $\delta < 1$ (and any modulus $L > 0$) since then any $\beta,\, \beta' \in \mathbb{B}^d_\delta[\bar\beta]$ satisfy

$$M(\beta) = \mathbb{B}_1(x^\infty) = M(\beta'),$$

which, via Lemma 3.5, results in a zero $\mathbf{d}$-distance on the left of (13).

On the other hand, the same basin mapping (2) is *not* **d**-Lipschitz continuous near $\bar{\beta} = 2$ (with any radius $\delta > 0$ or modulus $L > 0$), because any $\beta < 2$ has $M(\beta) = \mathbb{B}_1(x^\infty)$ while any $\beta' > 2$ has $M(\beta') = x^\infty$. For such pairs β and β', it follows that the **d**-distance on the left of (13) is 1, while the norm on the right side of (13) can be made arbitrarily small by choosing $\beta < 2$ and $\beta' > 2$ closer to $\bar{\beta} = 2$. Note that this same issue is why the radius δ of **d**-Lipschitz continuity near $\bar{\beta} = 1$ above must be smaller than 1.

3.1. d-Calmness

Calmness is a continuity property similar to Lipschitz continuity, but where only the base point $\bar{\beta}$ is required for comparison, in place of all $\beta' \in \mathbb{B}^d_\delta[\bar{\beta}] \cap \mathrm{dom}(M)$.

Definition 3.10. (**d**-Calm) For any pre-distance function **d**, we say the multiset-valued mapping M is **d**-*calm at* $\bar{\beta}$ if there exists a *radius* $\delta > 0$ and a *modulus* $L > 0$ such that

$$\mathbf{dist_d}\left(M(\beta), M(\bar{\beta})\right) \leq L \,\|\beta - \bar{\beta}\| \text{ for all } \beta \in \mathbb{B}^d_\delta[\bar{\beta}] \cap \mathrm{dom}(M). \tag{14}$$

Given a region $\Omega \subseteq \mathcal{X}$, we say that M is Ω-*truncated* **d**-*calm at* $\bar{\beta}$ if the truncated multiset-valued mapping $M_{\cap\Omega}(\beta) := M(\beta) \cap \Omega$ is **d**-calm at $\bar{\beta}$. □

Remark 3.11. (a) **d**-Calmness requires in particular that $\mathbf{dist_d}\left(M(\bar{\beta}), M(\bar{\beta})\right) = 0$.
(b) If $\bar{\beta} \in \mathrm{dom}(M)$ and a multiset-valued mapping M is **d**-Lipschitz continuous near $\bar{\beta}$ (Ω-truncated **d**-Lipschitz continuous near $\bar{\beta}$), then M is evidently also **d**-calm at $\bar{\beta}$ (Ω-truncated **d**-calm at $\bar{\beta}$), since $\beta' = \bar{\beta}$ is one possibility for comparison. □

Example 3.12. The basin mapping (2) from Examples 2.7 and 2.16 is **d**-calm at $\bar{\beta} = 1$ with radius $\delta < 1$ (and any modulus $L > 0$) since then any $\beta \in \mathbb{B}^d_\delta[\bar{\beta}]$ satisfies

$$M(\beta) = \mathbb{B}_1(x^\infty) = M(\bar{\beta}),$$

which, via Lemma 3.5, results in a zero **d**-distance on the left of (14). In addition, this mapping is **d**-calm at $\bar{\beta} = 1$ with any radius $\delta > 0$ and modulus $L \geq 1$, since $\beta \in \mathbb{B}^d_1(\bar{\beta})$ results in a zero **d**-distance on the left of (14) as above, while $\beta \in \mathbb{B}^d_\delta[\bar{\beta}] \setminus \mathbb{B}^d_1(\bar{\beta})$ results in the **d**-distance of one on the left side of (14) and a norm ≥ 1 on the right side.

On the other hand, the same basin mapping (2) is *not* **d**-calm at $\bar{\beta} = 2$ (with any radius $\delta > 0$ or modulus $L > 0$), because any $\beta < 2$ has $M(\beta) = \mathbb{B}_1(x^\infty)$ while $M(\bar{\beta}) = x^\infty$. It follows that the **d**-distance on the left of (14) is one, while the norm on the right side of (14) can be made arbitrarily small by choosing $\beta < 2$ closer to $\bar{\beta} = 2$. □

4. Grid continuity of multiset-valued mappings

Inspired by the (finite) sampling inherent in simulation, we define a new property of "grid continuity" where sampling is intrinsic. This property assumes that the range space is finite-dimensional $\mathcal{X} = \mathbb{R}^n$ (which covers basin mappings) and relies on the following construction:

1. consider a bounded sampling region $\Omega \subseteq \mathbb{R}^n$ of the range space (e.g., Figure 2.3 uses $\Omega = [-3, 3] \times [-3, 3] \subseteq \mathbb{R}^2$),

2. choose a (typically small) *mesh size* $\Delta > 0$, and
3. define the maximal regular grid Γ_Δ of points in Ω that are evenly spaced by Δ in each of the coordinate directions

$$\begin{aligned}\mathbf{e}_1 &= \overbrace{(1,0,0,\ldots,0,0)}^{n \text{ coordinates}},\\ \mathbf{e}_2 &= (0,1,0,\ldots,0,0),\\ &\vdots\\ \mathbf{e}_n &= (0,0,0,\ldots,0,1)\end{aligned}$$

(e.g., Figure 4.1 shows $\Gamma_{0.5}$ for $\Omega = [-3,3]\times[-3,3] \subseteq \mathbb{R}^2$).

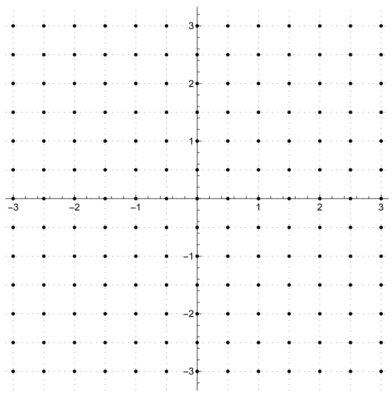

Figure 4.1: Grid $\Gamma_{0.5}$ for $\Omega = [-3,3]\times[-3,3] \subseteq \mathbb{R}^2$.

4.1. d-Lipschitz grid continuity

Our notion of grid continuity considers only outputs restricted to a maximal regular grid Γ_Δ and tests only inputs $\beta \in \mathbb{R}^d$ from the following discrete set of points:

$$B^d_{\bar\delta}[\bar\beta] := \left\{\bar\beta - \bar\delta\,\mathbf{e}_i,\ \bar\beta,\ \bar\beta + \bar\delta\,\mathbf{e}_i \,:\, \mathbf{e}_i \in \mathbb{R}^d\right\},$$

which is essentially a “grid-neighborhood” in $\mathbb{R}^d$ of radius $\bar\delta$ about the point $\bar\beta$.

Definition 4.1. (**d**-Lipschitz Γ_Δ-continuous) For any pre-distance function $\mathbf{d}$, we say that the multiset-valued mapping M is **d**-*Lipschitz* Γ_Δ-*continuous at* $\bar\beta$ *with radius* $\bar\delta > 0$ *and modulus* $L_{\bar\delta} > 0$ if

$$\mathbf{dist_d}\left(M_{\cap\Gamma_\Delta}(\beta), M_{\cap\Gamma_\Delta}(\beta')\right) \le L_{\bar\delta}\,\|\beta-\beta'\| \quad \text{for } \beta,\ \beta' \in B^d_{\bar\delta}[\bar\beta] \cap \mathrm{dom}(M_{\cap\Gamma_\Delta}). \tag{15}$$

Example 4.2. (**d**-Lipschitz Γ_Δ-continuous) We consider again the red basin mapping $M(\beta) = \epsilon\text{-Basin}_{\mathrm{AG},f_\beta}\left(x^\infty_\beta\right)$ defined by the ϵ-basins of attraction for I_{AG,f_β} from Example 2.17. In this case, the multisets all have cardinality $m = 1$, so the **d**-distance function on the left side of (15) satisfies

$$\begin{aligned}&\mathbf{dist_d}\big(M(\beta)\cap\Gamma_\Delta, M(\beta')\cap\Gamma_\Delta\big)\\ &= \max\Big\{\sup_{x\in M(\beta)\cap\Gamma_\Delta}\ \inf_{x'\in M(\beta')\cap\Gamma_\Delta}\|x-x'\|,\ \sup_{x'\in M(\beta')\cap\Gamma_\Delta}\ \inf_{x\in M(\beta)\cap\Gamma_\Delta}\|x'-x\|\Big\}.\end{aligned} \tag{16}$$

First, we'll use the radius $\bar{\delta} = 0.5$ and consider two different mesh sizes Δ for comparison.

$\beta = -1,\ \Delta = 0.5$ $\qquad$ $\beta = -0.5,\ \Delta = 0.5$ $\qquad$ $\beta = 0,\ \Delta = 0.5$

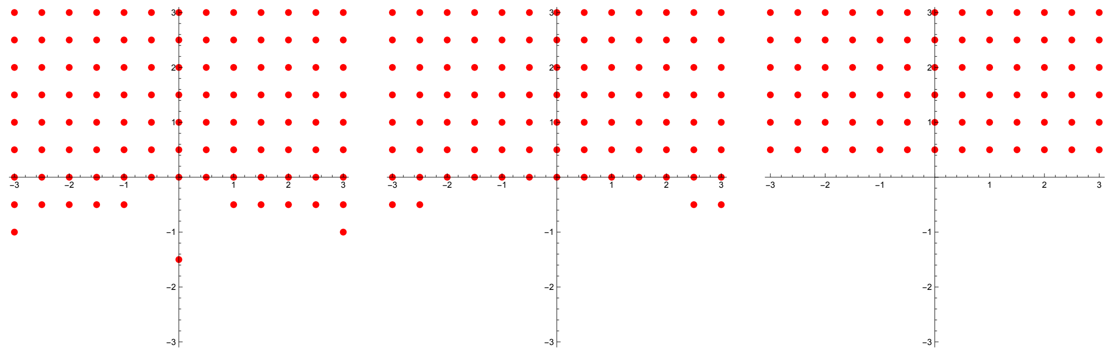

Figure 4.2: $M(\beta) \cap \Gamma_{0.5}$ at $\beta \in B^1_{0.5}[-0.5] = \{-1,\ -0.5,\ 0\}$.

$\boldsymbol{\Delta} = \mathbf{0.5}$: Figure 4.2 shows red dots for all the points in the intersections $M(\beta)\cap\Gamma_{0.5}$ and the three values of $\beta \in B^1_{0.5}[-0.5] = \{-1,\ -0.5,\ 0\}$. The data represented in Figure 4.2 yields the following values for the **d**-distance function (16) in this case:

$$\begin{aligned}
\mathbf{dist_d}\left(M(-1)\cap\Gamma_{0.5}, M(-0.5)\cap\Gamma_{0.5}\right) &= \|(0,-1.5)-(0,0)\| = 1.5,\\
\mathbf{dist_d}\left(M(-0.5)\cap\Gamma_{0.5}, M(0)\cap\Gamma_{0.5}\right) &= \|(3,-0.5)-(3,0.5)\| = 1,\\
\mathbf{dist_d}\left(M(-1)\cap\Gamma_{0.5}, M(0)\cap\Gamma_{0.5}\right) &= \|(0,-1.5)-(0,0.5)\| = 2,
\end{aligned} \tag{17}$$

and the **d**-distances between $M(\beta)\cap\Gamma_{0.5}$ and $M(\beta')\cap\Gamma_{0.5}$ are zero in this case whenever $\beta = \beta'$. The first **d**-distance in (17) corresponds to inputs β and β' satisfying $|\beta - \beta'| = 0.5$, which therefore requires a modulus $L_{\bar{\delta}} \geq 3$ in order to satisfy the Lipschitz bound (15). The second **d**-distance in (17) also corresponds to inputs β and β' satisfying $|\beta - \beta'| = 0.5$, but only requires a modulus $L_{\bar{\delta}} \geq 2$ in order to satisfy the Lipschitz bound (15). The last **d**-distance in (17) corresponds to inputs β and β' satisfying $|\beta-\beta'| = 1$, which therefore requires a modulus $L_{\bar{\delta}} \geq 2$ in order to satisfy the Lipschitz bound (15). We conclude that the red basin mapping $M(\beta) = \epsilon\text{-Basin}_{\mathrm{AG},f_\beta}\left(x^\infty_\beta\right)$ is **d**-Lipschitz $\Gamma_{0.5}$-continuous at $\bar{\beta} = -0.5$ with radius $\bar{\delta} = 0.5$ and modulus $L_{\bar{\delta}} = 3$.

$\boldsymbol{\Delta} = \mathbf{0.25}$: Figure 4.3 shows red dots for all points in the intersections $M(\beta)\cap\Gamma_{0.25}$ and the three values of $\beta \in B^1_{0.5}[-0.5] = \{-1,\ -0.5,\ 0\}$.

The data represented in Figure 4.3 yields the following values for the **d**-distance function (16) in this case:

$$\begin{aligned}
\mathbf{dist_d}\left(M(-1)\cap\Gamma_{0.25}, M(-0.5)\cap\Gamma_{0.25}\right) &= \|(0,-1.5)-(0,0)\| = 1.5,\\
\mathbf{dist_d}\left(M(-0.5)\cap\Gamma_{0.25}, M(0)\cap\Gamma_{0.25}\right) &= \|(3,-0.5)-(3,0.25)\| = 0.75,\\
\mathbf{dist_d}\left(M(-1)\cap\Gamma_{0.25}, M(0)\cap\Gamma_{0.25}\right) &= \|(0,-1.5)-(0,0.25)\| = 1.75,
\end{aligned} \tag{18}$$

and the **d**-distances between $M(\beta)\cap\Gamma_{0.25}$ and $M(\beta')\cap\Gamma_{0.25}$ are zero in this case whenever $\beta = \beta'$. The first **d**-distance in (18) corresponds to inputs β and β' satisfying $|\beta - \beta'| = 0.5$, which therefore requires a modulus $L_{\bar{\delta}} \geq 3$ in order to satisfy the Lipschitz bound (15). The second **d**-distance in (18) also corresponds to inputs β and β' satisfying $|\beta - \beta'| = 0.5$, but only requires a modulus $L_{\bar{\delta}} \geq 1.5$ in order to satisfy the Lipschitz bound (15). The last **d**-distance in (18) corresponds to inputs β and β' satisfying $|\beta - \beta'| = 1$, which therefore requires a modulus $L_{\bar{\delta}} \geq 1.75$ in order to satisfy the Lipschitz bound (15). We conclude that the red basin mapping $M(\beta) = \epsilon\text{-Basin}_{\mathrm{AG},f_\beta}\left(x_\beta^\infty\right)$ is **d**-Lipschitz $\Gamma_{0.25}$-continuous at $\bar{\beta} = -0.5$ with radius $\bar{\delta} = 0.5$ and modulus $L_{\bar{\delta}} = 3$.

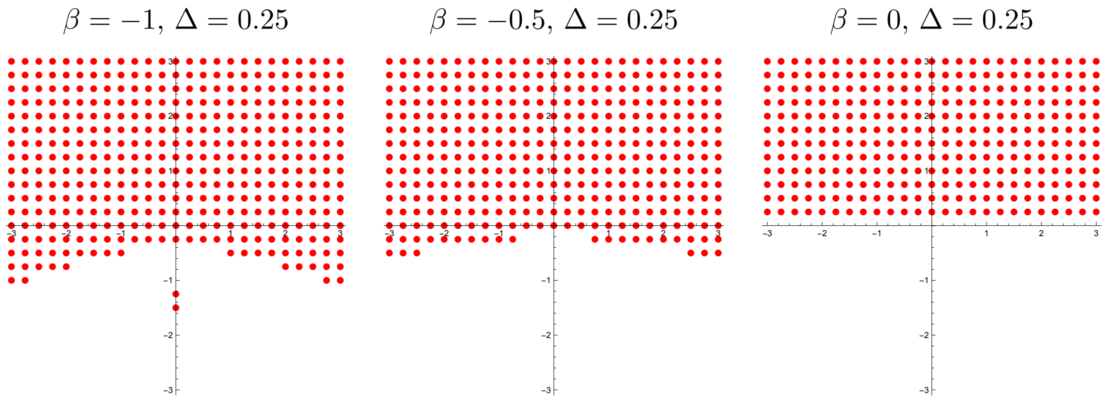

Figure 4.3: $M(\beta) \cap \Gamma_{0.25}$ at $\beta \in B^1_{0.5}[-0.5] = \{-1,\ -0.5,\ 0\}$.

Evidently decreasing the mesh size Δ from 0.5 to 0.25 in this example does not change the modulus, which confirms that these different mesh sizes don't reveal significantly new elements in the Ω-truncated images $M(\beta) \cap \Omega$ of the red basin mapping. If a smaller mesh size were to suddenly reveal a new (and relatively distant) "island" in $M(\beta) \cap \Omega$, we would see a change in the modulus $L_{\bar{\delta}}$.

Now we'll use the mesh size $\Delta = 0.25$ and consider two different radii $\bar{\delta}$ for comparison.

$\boldsymbol{\bar{\delta} = 0.5}$: This is the same as the second case above, where we determined the modulus $L_{\bar{\delta}} = 3$.

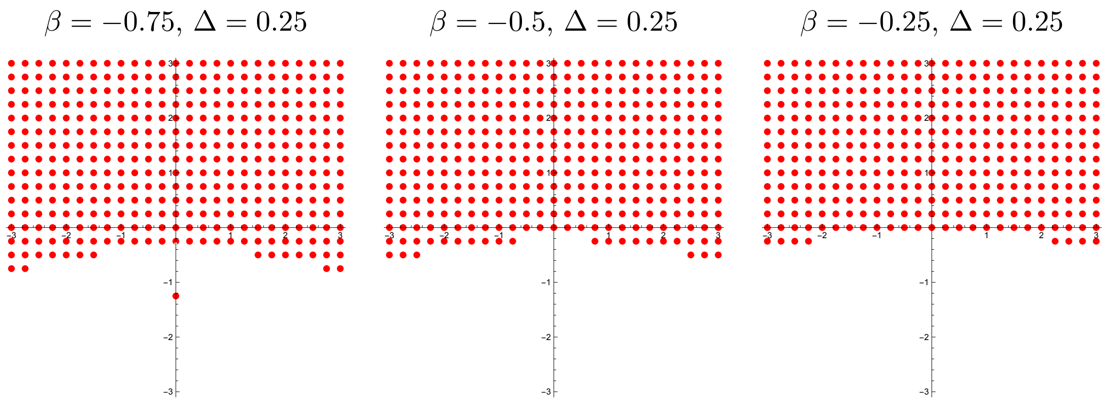

Figure 4.4: $M(\beta) \cap \Gamma_{0.25}$ at $\beta \in B^1_{0.25}[-0.5] = \{-0.75,\ -0.5,\ -0.25\}$.

$\boldsymbol{\bar{\delta} = 0.25}$: Figure 4.4 above shows red dots for all the points in the intersections $M(\beta) \cap \Gamma_{0.25}$ and the three values of $\beta \in B^1_{0.25}[-0.5] = \{-0.75,\ -0.5,\ -0.25\}$.

The data represented in Figure 4.4 yields the following values for the **d**-distance function (16) in this case:

$$\begin{aligned}
&\mathbf{dist_d}\left(M(-0.75)\cap\Gamma_{0.25}, M(-0.5)\cap\Gamma_{0.25}\right) = \|(0,-1.25)-(0,0)\| = 1.25,\\
&\mathbf{dist_d}\left(M(-0.5)\cap\Gamma_{0.25}, M(-0.25)\cap\Gamma_{0.25}\right) = \|(3,-0.5)-(3,-0.25)\| = 0.25, \quad (19)\\
&\mathbf{dist_d}\left(M(-0.75)\cap\Gamma_{0.25}, M(-0.25)\cap\Gamma_{0.25}\right) = \|(0,-1.25)-(0,0)\| = 1.25,
\end{aligned}$$

and the $\mathbf{d}$-distances between $M(\beta)\cap\Gamma_{0.25}$ and $M(\beta')\cap\Gamma_{0.25}$ are zero in this case whenever $\beta = \beta'$. The first $\mathbf{d}$-distance in (19) corresponds to inputs β and β' satisfying $|\beta-\beta'| = 0.25$, which therefore requires a modulus $L_{\bar\delta} \geq 5$ in order to satisfy the Lipschitz bound (15). The second $\mathbf{d}$-distance in (19) also corresponds to inputs β and β' satisfying $|\beta-\beta'| = 0.25$, but only requires a modulus $L_{\bar\delta} \geq 1$ in order to satisfy the Lipschitz bound (15). The last $\mathbf{d}$-distance in (19) corresponds to inputs β and β' satisfying $|\beta-\beta'| = 0.5$, which therefore requires a modulus $L_{\bar\delta} \geq 2.5$ in order to satisfy the Lipschitz bound (15). We conclude that the red basin mapping $M(\beta) = \epsilon\text{-Basin}_{\mathrm{AG},f_\beta}\left(x_\beta^\infty\right)$ is $\mathbf{d}$-Lipschitz $\Gamma_{0.25}$-continuous at $\bar\beta = -0.5$ with radius $\bar\delta = 0.25$ and modulus $L_{\bar\delta} = 5$.

Evidently decreasing the radius $\bar\delta$ from 0.5 to 0.25 in this example increases the modulus from 3 to 5. □

Remark 4.3. Notice that we can always confirm grid continuity in this manner because there are only a finite number of β and β' values to check in order to confirm the Lipschitz bound (15) (whose left side we can also compute because the grid Γ_Δ has only a finite number of points to check). For the same reason, mappings like this will always be grid continuous for *some* (large enough) modulus.

4.2. Truncated d-Lipschitz continuity implies d-Lipschitz grid continuity

The following theorem formalizes the relationship between the moduli for truncated $\mathbf{d}$-Lipschitz continuity and $\mathbf{d}$-Lipschitz grid continuity.

Theorem 4.4. (truncated $\mathbf{d}$-Lipschitz $\implies$ $\mathbf{d}$-Lipschitz grid continuity) *Suppose a multiset-valued mapping M is Ω-truncated $\mathbf{d}$-Lipschitz continuous near $\bar\beta$ with radius $\delta > 0$ and modulus $L > 0$. Then, for any radius $\bar\delta \leq \delta$ and mesh size $\Delta > 0$, M is $\mathbf{d}$-Lipschitz Γ_Δ-continuous at $\bar\beta$ with radius $\bar\delta$ and modulus $L_{\bar\delta} = L + \max\{\gamma'_{\bar\delta,\Delta}, 0\}$, where*

$$\gamma'_{\bar\delta,\Delta} := \max_{\beta\neq\beta'\in B^d_{\bar\delta}[\bar\beta]\cap\mathrm{dom}\left(M_{\cap\Gamma_\Delta}\right)} \frac{1}{\bar\delta}\left(\mathbf{dist_d}\left(M_{\cap\Gamma_\Delta}(\beta), M_{\cap\Gamma_\Delta}(\beta')\right) - \mathbf{dist_d}\left(M_{\cap\Omega}(\beta), M_{\cap\Omega}(\beta')\right)\right). \quad (20)$$

Proof. Since $\Gamma_\Delta \subseteq \Omega$, we know that $M_{\cap\Gamma_\Delta}(\beta) \subseteq M_{\cap\Omega}(\beta)$ for all $\beta \in \mathbb{R}^d$ and, consequently, that $\mathrm{dom}\left(M_{\cap\Gamma_\Delta}\right) \subseteq \mathrm{dom}\left(M_{\cap\Omega}\right)$. From this and the fact that $B^d_{\bar\delta}[\bar\beta] \subseteq \mathbb{B}^d_\delta[\bar\beta]$ (since $\bar\delta \leq \delta$), we deduce, from the assumption of Ω-truncated $\mathbf{d}$-Lipschitz continuity near $\bar\beta$, that every pair of β, $\beta' \in B^d_{\bar\delta}[\bar\beta] \cap \mathrm{dom}\left(M_{\cap\Gamma_\Delta}\right)$ satisfies the inequality

$$\mathbf{dist_d}\left(M_{\cap\Omega}(\beta), M_{\cap\Omega}(\beta')\right) \leq L\,\|\beta-\beta'\|. \quad (21)$$

In the special case that $\beta = \beta'$, the bound (21) implies $\mathbf{dist_d}\left(M_{\cap\Omega}(\beta), M_{\cap\Omega}(\beta)\right) = 0$ which, by Lemma 3.5, implies that

$$M_{\cap\Omega}(\beta) = \mathbf{d}\text{-cl}\ M_{\cap\Omega}(\beta) = \left\{\bar X : \inf_{X\in M_{\cap\Omega}(\beta)} \mathbf{d}\left(X,\bar X\right) = 0\right\}.$$

It follows that

$$M_{\cap\Gamma_\Delta}(\beta) = M_{\cap\Omega}(\beta) \cap \Gamma_\Delta = \mathbf{d}\text{-cl } M_{\cap\Omega}(\beta) \cap \Gamma_\Delta = \Big\{ \bar{X} \in \Gamma_\Delta : \inf_{X \in M_{\cap\Omega}(\beta)} \mathbf{d}\left(X, \bar{X}\right) = 0 \Big\}. \quad (22)$$

We also have (by definition of **d**-closure) that

$$\mathbf{d}\text{-cl } M_{\cap\Gamma_\Delta}(\beta) := \Big\{ \bar{X} : \inf_{X \in M_{\cap\Gamma_\Delta}(\beta)} \mathbf{d}\left(X, \bar{X}\right) = 0 \Big\} = \Big\{ \bar{X} : \min_{X \in M_{\cap\Gamma_\Delta}(\beta)} \mathbf{d}\left(X, \bar{X}\right) = 0 \Big\},$$

where the second equality follows since Γ_Δ is a discrete set. In consequence, for any $\bar{X} \in \mathbf{d}$-cl $M_{\cap\Gamma_\Delta}(\beta)$, there exists an $X \in M_{\cap\Gamma_\Delta}(\beta)$ with $\mathbf{d}\left(X, \bar{X}\right) = 0$. Since $M_{\cap\Gamma_\Delta}(\beta) \subseteq M_{\cap\Omega}(\beta)$, we conclude from (22) above that $\bar{X} \in M_{\cap\Gamma_\Delta}(\beta)$. Since $\bar{X} \in \mathbf{d}$-cl $M_{\cap\Gamma_\Delta}(\beta)$ is arbitrary, we have $\mathbf{d}$-cl $M_{\cap\Gamma_\Delta}(\beta) \subseteq M_{\cap\Gamma_\Delta}(\beta)$, so that $M_{\cap\Gamma_\Delta}(\beta)$ is **d**-closed. Appealing again to Lemma 3.5, we have $\mathbf{dist_d}\left(M_{\cap\Gamma_\Delta}(\beta), M_{\cap\Gamma_\Delta}(\beta)\right) = 0$, which evidently satisfies the claimed **d**-Lipschitz Γ_Δ-continuity bound

$$\mathbf{dist_d}\left(M_{\cap\Gamma_\Delta}(\beta), M_{\cap\Gamma_\Delta}(\beta')\right) \leq \left(L + \max\{\gamma'_{\bar{\delta},\Delta}, 0\}\right) \|\beta - \beta'\| \quad (23)$$

for $\beta' = \beta$. Thus, we need only consider $\beta \neq \beta'$.

If $\gamma'_{\bar{\delta},\Delta} \leq 0$, then its definition (20) implies that

$$\mathbf{dist_d}\left(M_{\cap\Gamma_\Delta}(\beta), M_{\cap\Gamma_\Delta}(\beta')\right) \leq \mathbf{dist_d}\left(M_{\cap\Omega}(\beta), M_{\cap\Omega}(\beta')\right),$$

and the claimed **d**-Lipschitz Γ_Δ-continuity bound (23) is satisfied via (21).

To address the remaining case, we proceed by contradiction and suppose that there exists a radius $\bar{\delta} \leq \delta$ and a mesh size $\Delta > 0$, as well as a pair $\beta \neq \beta'$ from $B^d_{\bar{\delta}}[\bar{\beta}] \cap \operatorname{dom}(M_{\cap\Gamma_\Delta})$, for which the $\gamma'_{\bar{\delta},\Delta}$ defined by (20) is positive and M satisfies

$$\mathbf{dist_d}\left(M_{\cap\Gamma_\Delta}(\beta), M_{\cap\Gamma_\Delta}(\beta')\right) > (L + \gamma'_{\bar{\delta},\Delta}) \|\beta - \beta'\|. \quad (24)$$

Since $\beta \neq \beta'$ are both in $B^d_{\bar{\delta}}[\bar{\beta}]$, we know $\|\beta - \beta'\| \geq \bar{\delta}$. Combining this with the bounds (21) and (24) gives

$$\mathbf{dist_d}\left(M_{\cap\Gamma_\Delta}(\beta), M_{\cap\Gamma_\Delta}(\beta')\right) > \mathbf{dist_d}\left(M_{\cap\Omega}(\beta), M_{\cap\Omega}(\beta')\right) + \gamma'_{\bar{\delta},\Delta}\, \bar{\delta},$$

which contradicts the definition (20) of $\gamma'_{\bar{\delta},\Delta}$. □

4.2.1. d-Lipschitz grid continuity $\not\Rightarrow$ truncated d-Lipschitz continuity

A reverse implication to that in Theorem 4.4 might be stated as follows:

> If there exists $\delta > 0$ such that for any radius $\bar{\delta} \leq \delta$ and mesh size $\Delta > 0$, the multiset-valued mapping M is **d**-Lipschitz Γ_Δ-continuous at $\bar{\beta}$ with radius $\bar{\delta}$ and modulus $L_{\bar{\delta}}$, then M is be Ω-truncated **d**-Lipschitz continuous near $\bar{\beta}$ with radius $\delta > 0$ and modulus
>
> $$L := \sup_{\bar{\delta} \in (0,\delta]\,\&\,\Delta > 0} L_{\bar{\delta}} - \max\{\gamma'_{\bar{\delta},\Delta}, 0\}.$$

However, this statement is not true, as the following example shows.

Example 4.5. Consider the simple mapping M on $\mathbb{R}^2$ defined by

$$M(\beta_1,\beta_2)=\begin{cases}0 & \text{if } \beta_1\,\beta_2=0\\ 1 & \text{otherwise.}\end{cases}$$

If we choose $\bar\beta=(0,0)$ and $\Omega=[-1,1]\subseteq\mathbb{R}$, M is *not* Ω-truncated $\mathbf{d}$-Lipschitz continuous near $\bar\beta$ for any radius $\delta>0$ and modulus L. This follows because for any $\nu\in\mathbb{N}^+$, the points $\beta_\nu:=\left(\frac{1}{\nu},\frac{1}{\nu}\right)$ and $\beta'=\bar\beta$ satisfy

$$\mathbf{dist_d}\left(M_{\cap\Omega}(\beta_\nu),M_{\cap\Omega}(\beta')\right)=1 \quad\text{and}\quad \|\beta_\nu-\beta'\|=\frac{\sqrt{2}}{\nu},$$

and by increasing ν we can ensure both that $\beta_\nu\in\mathbb{B}^2_\delta[\bar\beta]$, and that the Lipschitz bound in (13) is not satisfied.

On the other hand, the mapping M is identically zero at any point β in the grid-neighborhood

$$B^2_{\bar\delta}[\bar\beta]=\{(-\bar\delta,0),(0,-\bar\delta),(0,0),(\bar\delta,0),(0,\bar\delta)\},$$

so M is trivially $\mathbf{d}$-Lipschitz Γ_Δ-continuous at $\bar\beta$, for any grid Γ_Δ.

4.3. d-Calm grid continuity

Since calmness only requires the base point $\bar\beta$ for comparison, we can confirm our $\mathbf{d}$-calm analogue of grid continuity from fewer computations than are generally required to confirm $\mathbf{d}$-Lipschitz grid continuity.

Definition 4.6. ($\mathbf{d}$-calm Γ_Δ-continuous) For any pre-distance function $\mathbf{d}$, we say that the multiset-valued mapping M is $\mathbf{d}$-*calm* Γ_Δ-*continuous at* $\bar\beta$ *with radius* $\bar\delta>0$ *and modulus* $L_{\bar\delta}>0$ if

$$\mathbf{dist_d}\left(M_{\cap\Gamma_\Delta}(\beta),M_{\cap\Gamma_\Delta}(\bar\beta)\right)\le L_{\bar\delta}\,\|\beta-\bar\beta\| \quad\text{for all } \beta\in B^d_{\bar\delta}[\bar\beta]\cap\operatorname{dom}(M_{\cap\Gamma_\Delta}). \tag{25}$$

Remark 4.7. The work we did in from Example 4.2 (requiring only the first two distances in each of (17), (18), and (19)) shows that the red basin mapping $M(\beta)=\epsilon\text{-Basin}_{\mathrm{AG},f_\beta}\left(x^\infty_\beta\right)$ is

- $\mathbf{d}$-calm $\Gamma_{0.5}$-continuous at $\bar\beta=-0.5$ with radius $\bar\delta=0.5$ and modulus $L_{\bar\delta}=3$,
- $\mathbf{d}$-calm $\Gamma_{0.25}$-continuous at $\bar\beta=-0.5$ with radius $\bar\delta=0.5$ and modulus $L_{\bar\delta}=3$,
- $\mathbf{d}$-calm $\Gamma_{0.25}$-continuous at $\bar\beta=-0.5$ with radius $\bar\delta=0.25$ and modulus $L_{\bar\delta}=5$.

The following companion to Theorem 4.4 is proved via the same argument there, but with β' replaced by $\bar\beta$.

Theorem 4.8. (truncated $\mathbf{d}$-calm $\Longrightarrow$ $\mathbf{d}$-calm grid continuity) *Suppose a multiset-valued mapping M is Ω-truncated* $\mathbf{d}$-*calm near $\bar\beta$ with radius $\delta>0$ and modulus $L>0$. Then, for any radius $\bar\delta\le\delta$ and mesh size $\Delta>0$, M is* $\mathbf{d}$-*calm Γ_Δ-continuous at $\bar\beta$ with radius $\bar\delta$ and modulus $L_{\bar\delta}=L+\max\{\gamma_{\bar\delta,\Delta},0\}$, where*

$$\gamma_{\bar\delta,\Delta}:=\max_{\beta\in B^d_{\bar\delta}[\bar\beta]\cap\operatorname{dom}\left(M_{\cap\Gamma_\Delta}\right)}\frac{1}{\bar\delta}\Big(\mathbf{dist_d}\left(M_{\cap\Gamma_\Delta}(\beta),M_{\cap\Gamma_\Delta}(\bar\beta)\right)-\mathbf{dist_d}\left(M_{\cap\Omega}(\beta),M_{\cap\Omega}(\bar\beta)\right)\Big). \tag{26}$$

5. Pre-processing via simulation

Theorem 4.4 explicitly links grid-continuity moduli to truncated **d**-Lipschitz moduli, which suggests that we might use simulations to investigate **d**-Lipschitz grid continuity prior to attempting to demonstrate truncated **d**-Lipschitz continuity of basin mappings analytically. The following rubric is based on our investigation in Example 4.2.

Pre-processing truncated d-Lipschitz continuity via d-Lipschitz grid continuity.

1. Fix the radius $\bar{\delta}$ and choose a mesh size Δ. Then decrease the mesh size Δ until a stable lower bound is observed on the **d**-Lipschitz grid-continuity modulus $L_{\bar{\delta}}$ (signaling that even smaller mesh sizes won't reveal significant new features). Fix that mesh size.
2. Decrease the radius $\bar{\delta}$ while computing $L_{\bar{\delta}}$, and the value $\gamma'_{\bar{\delta},\Delta}$ from (20).
3. Determine the prospective value of the Ω-truncated **d**-Lipschitz modulus by computing the difference $L_{\bar{\delta}} - \gamma'_{\bar{\delta},\Delta}$.
   - If the difference $L_{\bar{\delta}} - \gamma'_{\bar{\delta},\Delta}$ is consistent across the different $\bar{\delta}$, expect that the mapping is Ω-truncated **d**-Lipschitz continuous with modulus $L = L_{\bar{\delta}} - \gamma'_{\bar{\delta},\Delta}$.
   - If the difference $L_{\bar{\delta}} - \gamma'_{\bar{\delta},\Delta}$ is not consistent across the different $\bar{\delta}$, expect that the mapping fails to be Ω-truncated **d**-Lipschitz continuous.

Remark 5.1. The calculation of $\gamma'_{\bar{\delta},\Delta}$ from (20) in step 2 requires us to work directly with the truncated mapping $M_{\cap\Omega}$ for each value of $\bar{\delta}$, in order to compute $\mathbf{dist_d}\left(M_{\cap\Omega}(\beta), M_{\cap\Omega}(\beta')\right)$. However, there are only a finite number of images $M_{\cap\Omega}(\beta)$ and $M_{\cap\Omega}(\beta')$ to consider since $\beta \neq \beta' \in B^d_{\bar{\delta}}[\bar{\beta}]$, so this requirement is generally feasible. $\square$

To see how this approach works in practice, we'll now explore a few examples.

$\beta = -0.5$ $\beta = 0$ $\beta = 0.5$

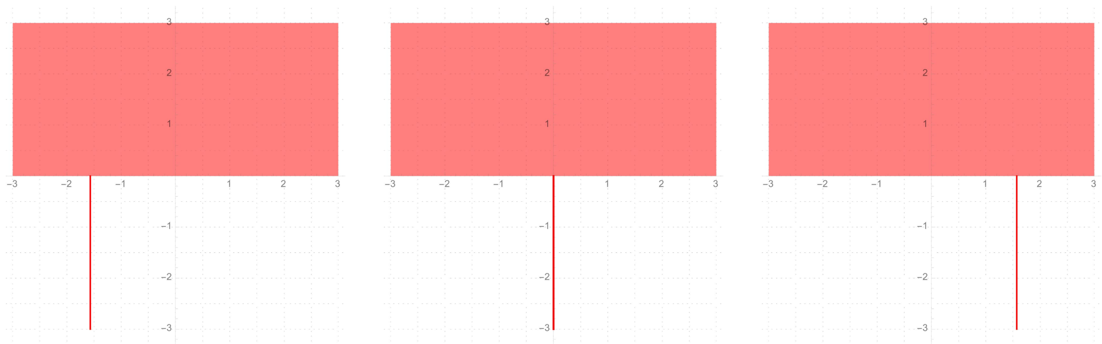

Figure 5.1: $M_{\cap\Omega}(\beta)$ at various β

Example 5.2. We consider the region

$$\Omega := \{(x_1, x_2) : -3 \leq x_1 \leq 3 \ \ \& \ -3 \leq x_2 \leq 3\}$$

and the mapping M defined by

$$M(\beta) = \{(x_1, x_2) : x_2 \geq 0\} \cup \{(x_1, x_2) : x_1 = \pi\,\beta\}. \tag{27}$$

Figure 5.1 shows three representative plots of images of the resulting truncated mapping $M_{\cap\Omega}$.

(1) Since π is irrational, the vertical lines $x_1 = \pi\,\beta$ will not intersect the grid $\Gamma_{\frac{1}{\nu}}$ for any $\beta \in \mathbb{Q} \setminus \{0\}$ and any $\nu \in \mathbb{N}^+$. This is illustrated in Figure 5.2 showing plots of three representative images of the grid-restricted mapping $M_{\Gamma_{\frac{1}{2}}}(\beta)$, demonstrating that the grid-restricted mapping $M_{\cap\Gamma_{\frac{1}{\nu}}}$ satisfies

$$\begin{aligned}&\mathbf{dist_d}\left(M_{\cap\Gamma_{\frac{1}{\nu}}}(\beta), M_{\cap\Gamma_{\frac{1}{\nu}}}(0)\right)\\ &= \max\left\{\sup_{x\in M_{\cap\Gamma_{\frac{1}{\nu}}}(\beta)}\ \inf_{x'\in M_{\cap\Gamma_{\frac{1}{\nu}}}(0)} \|x - x'\|,\ \sup_{x'\in M_{\cap\Gamma_{\frac{1}{\nu}}}(0)}\ \inf_{x\in M_{\cap\Gamma_{\frac{1}{\nu}}}(\beta)} \|x' - x\|\right\} = 3\end{aligned}$$

for any $\beta \in \mathbb{Q} \setminus \{0\}$ and any $\nu \in \mathbb{N}^+$, since 3 is the gap between the upper half-plane and the point $(0, -3) \in M_{\cap\Gamma_{\frac{1}{\nu}}}(0)$ on the x_2-axis.

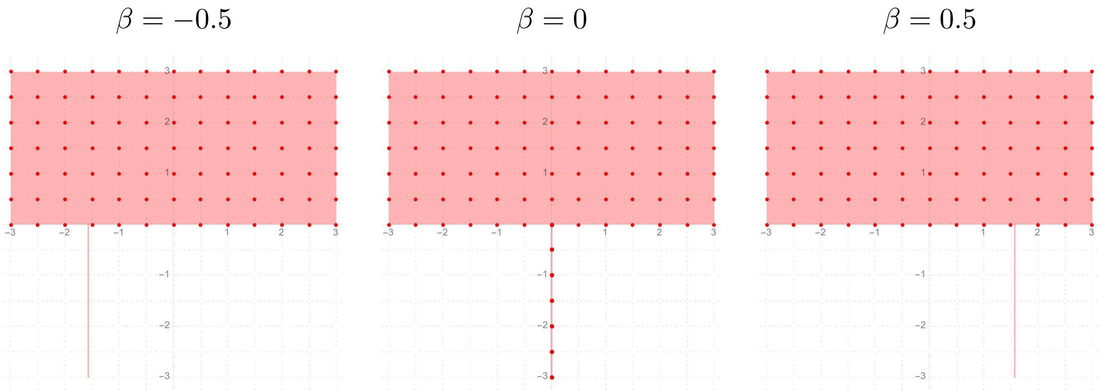

Figure 5.2: $M_{\Gamma_{\frac{1}{2}}}(\beta)$ at various β

It follows that if we use mesh size $\Delta = \frac{1}{\nu}$ and increase ν (to decrease Δ) while fixing the radius $\bar{\delta}$, we will see a stable modulus $L_{\bar{\delta}} = \frac{3}{\bar{\delta}}$. We thus can fix the mesh size $\Delta = \frac{1}{2}$.

(2) For any choice of radius $\bar{\delta}$, we have modulus $L_{\bar{\delta}} = \frac{3}{\bar{\delta}}$ and, via (20),

$$\gamma'_{\bar{\delta},\frac{1}{2}} = \frac{3 - \pi\,\bar{\delta}}{\bar{\delta}} = L_{\bar{\delta}} - \pi.$$

(3) The difference $L_{\bar{\delta}} - \gamma'_{\bar{\delta},\frac{1}{2}}$ in this case is π, which doesn't change at all as $\bar{\delta}$ is decreased, so we expect that M is Ω-truncated **d**-Lipschitz continuous near $\bar{\beta} = 0$ with modulus $L = \pi$.

In this case, we can demonstrate that the truncated mapping $M_{\cap\Omega}$ satisfies

$$\begin{aligned}&\mathbf{dist_d}\left(M_{\cap\Omega}(\beta), M_{\cap\Omega}(\beta')\right)\\ &= \max\left\{\sup_{x\in M_{\cap\Omega}(\beta)}\ \inf_{x'\in M_{\cap\Omega}(\beta')} \|x - x'\|,\ \sup_{x'\in M_{\cap\Omega}(\beta')}\ \inf_{x\in M_{\cap\Omega}(\beta)} \|x' - x\|\right\} = \pi\,|\beta - \beta'|,\end{aligned}$$

since the largest gap occurs between the vertical lines $x_1 = \pi\,\beta$ and $x_1 = \pi\,\beta'$. Thus M is indeed Ω-truncated $\mathbf{d}$-Lipschitz continuous near $\bar{\beta} = 0$ with any radius $\delta > 0$ and with modulus $L = \pi$. □

Remark 5.3. Note that the grid-continuity modulus $L_{\bar{\delta}} = \frac{3}{\bar{\delta}}$ in this example approaches infinity as the radius $\bar{\delta}$ approaches zero. □

Example 5.2 illustrates how pre-processing might work when the mapping M is $\mathbf{d}$-Lipschitz continuous, and next we'll explore an example where this appears to not be the case.

Example 5.4. We revisit the red basin mapping $M(\beta) = \epsilon\text{-Basin}_{\mathrm{AG},f_\beta}\left(x_\beta^\infty\right)$ defined by the ϵ-basins of attraction for I_{AG,f_β} from Examples 2.17 and 4.2.

(1) If we fix the radius $\bar{\delta} = 0.5$, the first part of Example 4.2 shows us that decreasing the mesh size Δ from 0.5 to 0.25 does not change the lower bound on the $\mathbf{d}$-Lipschitz grid-continuity modulus $L_{\bar{\delta}} = 3$, so we fix $\Delta = 0.25$.

(2) In the second part of Example 4.2, we computed $L_{0.5} = 3$ and $L_{0.25} = 5$. Evidently, to compute $\gamma'_{\bar{\delta},\Delta}$ from (20), we need to evaluate $\mathbf{dist_d}\left(M_{\cap\Omega}(\beta), M_{\cap\Omega}(\beta')\right)$ for $\beta \neq \beta' \in B^d_{\bar{\delta}}[\bar{\beta}]$.

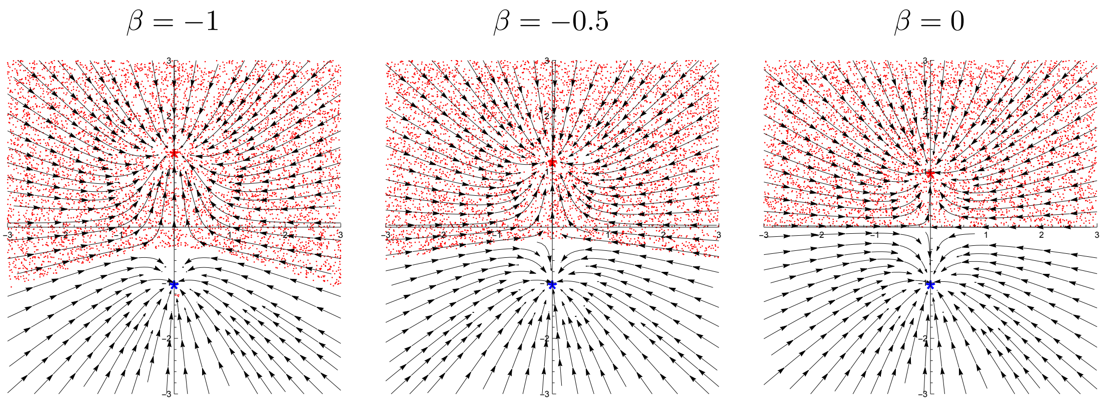

Figure 5.3: $M(\beta) \cap \Omega$ at $\beta \in B^1_{0.5}[-0.5] = \{-1,\ -0.5,\ 0\}$.

Fig. 5.3 shows plots of simulated images $M(\beta)\cap\Omega$ for $\beta \in B^1_{0.5}[-0.5] = \{-1,\ -0.5,\ 0\}$, and we used the data represented there to compute the following values:

$$\begin{aligned}
\mathbf{dist_d}\left(M_{\cap\Omega}(-1), M_{\cap\Omega}(-0.5)\right) &= 0.93602 \\
\mathbf{dist_d}\left(M_{\cap\Omega}(-0.5), M_{\cap\Omega}(0)\right) &= 0.562199 \\
\mathbf{dist_d}\left(M_{\cap\Omega}(-1), M_{\cap\Omega}(0)\right) &= 1.49822.
\end{aligned}$$

These values, and those in (18) allow us to compute the following value of $\gamma'_{0.5,0.25}$ associated with the radius $\bar{\delta} = 0.5$ and mesh size $\Delta = 0.25$:

$$\gamma'_{0.5,0.25} = \max\left\{\frac{1.5 - 0.93602}{0.5}, \frac{0.75 - 0.562199}{0.5}, \frac{1.75 - 1.49822}{0.5}\right\} = 1.12796.$$

Figure 5.4 shows plots of simulated images $M(\beta) \cap \Omega$ for

$$\beta \in B^1_{0.25}[-0.5] = \{-0.75,\ -0.5,\ -0.25\},$$

and we used the data represented there to compute the following values:

$$\begin{aligned}\mathbf{dist_d}\left(M_{\cap\Omega}(-0.75), M_{\cap\Omega}(-0.5)\right) &= 0.692696\\ \mathbf{dist_d}\left(M_{\cap\Omega}(-0.5), M_{\cap\Omega}(-0.25)\right) &= 0.257909\\ \mathbf{dist_d}\left(M_{\cap\Omega}(-0.75), M_{\cap\Omega}(-0.25)\right) &= 0.950605.\end{aligned}$$

$\beta = -0.75$ $\beta = -0.5$ $\beta = -0.25$

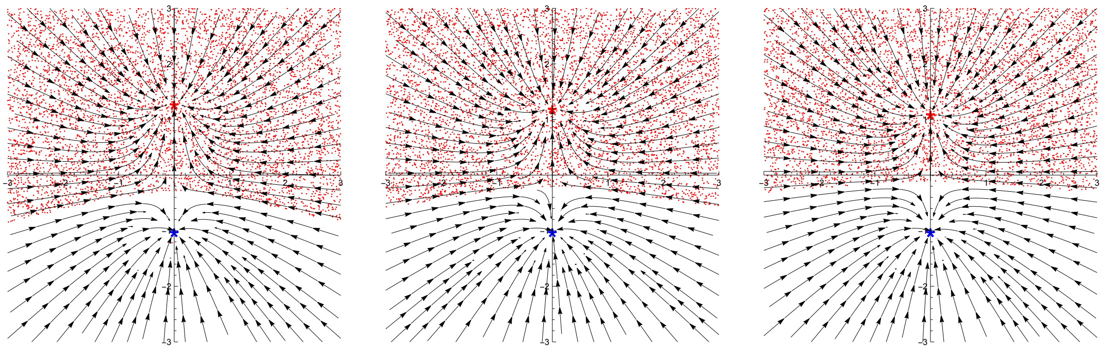

Figure 5.4: $M(\beta) \cap \Omega$ at $\beta \in B^1_{0.25}[-0.5] = \{-0.75, -0.5, -0.25\}$.

These values, and those in (19) allow us to compute the following value of $\gamma'_{0.25,0.25}$ associated with the radius $\bar{\delta} = 0.25$ and mesh size $\Delta = 0.25$:

$$\gamma'_{0.25,0.25} = \max\left\{\frac{1.25 - 0.692696}{0.25}, \frac{0.25 - 0.257909}{0.25}, \frac{1.25 - 0.950605}{0.25}\right\} = 2.22922.$$

We have the following equations for the prospective modulus L if the red basin mapping was Ω-truncated $\mathbf{d}$-Lipschitz near $\bar{\beta} = -0.5$:

$$L_{0.5} - \gamma'_{0.5,0.25} = 3 - 0.950605 = 2.0494 \text{ and } L_{0.25} - \gamma'_{0.25,0.25} = 5 - 2.22922 = 2.77078.$$

These are not consistent, so we expect that the red basin mapping fails to be Ω-truncated $\mathbf{d}$-Lipschitz near $\bar{\beta} = -0.5$.

According to Figures 2.3 and 2.4, the red basin mapping $M(\beta) = \epsilon\text{-Basin}_{\mathrm{AG},f_\beta}\left(x^\infty_\beta\right)$ indeed appears to fail to be $\mathbf{d}$-Lipschitz continuous near $\bar{\beta} = -0.5$ (for any radius $\delta > 0$ and modulus $L > 0$). This follows since the red island of points about $(0, -1.225)$ does not appear in $M(\beta')$ when $\beta' \geq -0.5$. Thus, the closest point to $(0, -1.225)$ in $M(\beta')$ for $\beta' \geq -0.5$ is the saddle at $\left(0, \frac{1}{2}\left(1 - \sqrt{1 - 2\beta'}\right)\right)$. Moreover, the point $(0, -1.225)$ is in $M(\beta)$ when $\beta < -0.5$. We conclude that the $\mathbf{d}$-distance on the left side of the inequality in (13) in this case satisfies

$$\mathbf{dist_d}\left(M(\beta), M(\beta')\right) \geq 0.5\left|\sqrt{1 - 2\beta'} - 3.45\right| \approx 1$$

for $\beta < -0.5 \leq \beta'$ close to -0.5, while the right side of the inequality in (13) is approximately zero when β' and β are both close to $\bar{\beta} = -0.5$.

Notice that Figure 2.3 covers the region $\Omega = [-3, 3] \times [-3, 3] \subseteq \mathbb{R}^2$ so we also can say that the basin mapping M also appears to fail to be Ω-truncated $\mathbf{d}$-Lipschitz continuous near $\bar{\beta} = -0.5$.

Remark 5.5. Notice that the $\gamma'_{\bar{\delta},\Delta}$ in both Examples 5.2 and 5.4 increase as the radius $\bar{\delta}$ decreases. In Example 5.2, all of the increase in $\gamma'_{\bar{\delta},\Delta}$ is due to the increasing **d**-Lipschitz grid-continuity modulus $L_{\bar{\delta}}$, but in Example 5.4, some of this increase was due to an increasing prospective modulus L (signaling that there indeed is no modulus L). These two examples illustrate that an increasing **d**-Lipschitz grid-continuity modulus alone is not enough to make conclusions about the **d**-Lipschitz continuity of a mapping. □

We can also use the following approach, inspired by Theorem 4.8, to pre-process truncated **d**-calmness via **d**-calm grid continuity.

Pre-processing truncated d-calmness via d-calm grid continuity.

1. Fix the radius $\bar{\delta}$ and choose a mesh size Δ sufficient for the scale of the particular problem. Then decrease the mesh size Δ until a stable lower bound is observed on the **d**-calm grid-continuity modulus $L_{\bar{\delta}}$ (signaling that even smaller mesh sizes won't reveal significant new features). Fix that mesh size.
2. Decrease the radius $\bar{\delta}$ while computing $L_{\bar{\delta}}$, and the value $\gamma_{\bar{\delta},\Delta}$ from (26).
3. Determine the prospective value of the Ω-truncated **d**-calm modulus by computing the difference $L_{\bar{\delta}} - \gamma_{\bar{\delta},\Delta}$.
   - If the difference $L_{\bar{\delta}} - \gamma_{\bar{\delta},\Delta}$ is consistent across the different $\bar{\delta}$, expect that the mapping *is* Ω-truncated **d**-calm with modulus $L = L_{\bar{\delta}} - \gamma_{\bar{\delta},\Delta}$.
   - If the difference $L_{\bar{\delta}} - \gamma_{\bar{\delta},\Delta}$ is not consistent across the different $\bar{\delta}$, expect that the mapping *is not* Ω-truncated **d**-calm.

Remark 5.6. Examples 5.2, 5.4, and 4.5 all show the same conclusions about **d**-calmness as they did for **d**-Lipschitz continuity, while requiring fewer calculations than were used in those examples. For instance, to compute $\gamma_{\bar{\delta},\Delta}$ from (26), in order to determine **d**-calmness, requires $2\,(2^d+1)$ **d**-distance calculations (since there are 2^d+1 elements in $B^d_{\bar{\delta}}[\bar{\beta}]$, and two **d**-distances to compute in the numerator of (26)). This compares favorably to the

$$2\left((2^d+1)+2^d+(2^d-1)+\ldots+1\right) = (2^d+2)(2^d+1)$$

d-distance calculations required to compute $\gamma'_{\bar{\delta},\Delta}$ from (20) in order to determine **d**-Lipschitz continuity.

References

[1] P.-A. Absil, K. Kurdyka: *On the stable equilibrium points of gradient systems*, Systems Control Letters 55 (2006) 573–577.

[2] D. Asenjo, J. D. Stevenson, D. J. Wales, D. Frenkel: *Visualizing basins of attraction for different minimization algorithms*, J. Phys. Chem. B 117 (2013) 12717–12723.

[3] A. S. Bosman, A. Engelbrecht, M. Helbig: *Visualising basins of attraction for the cross-entropy and the squared error neural network loss functions*, arXiv: 1901.02302 (2019).

[4] P. Brzeski, P. Belardinelli, S. Lenci, P. Perlikowski: *Revealing compactness of basins of attraction of multi-DoF dynamical systems*, Mech. Syst. Signal Processing 111 (2018) 348–361.

[5] M.-F. Danca, P. Bourke, N. Kuznetsov: *Graphical structure of attraction basins of hidden chaotic attractors: The Rabinovich-Fabrikant system*, Int. J. Bifurcation Chaos 29 (2019), art. no. 1930001.

[6] A. Daza, A. Wagemakers, B. Georgeot, D. Guéry-Odelin, M.A.F. Sanjuán: *Basin entropy: a new tool to analyze uncertainty in dynamical systems*, Sci. Rep. 6 (2016), art. no. 31416.

[7] Z. Faghani, Z. Arab, F. Parastesh, S. Jafari, M. Perc, M. Slavinec: *Effects of different initial conditions on the emergence of chimera states*, Chaos Solitons Fractals 114 (2018) 306–311.

[8] A. B. Levy: *Attraction in Numerical Minimization*, Springer Briefs in Optimization, Springer, Cham (2018).

[9] A. B. Levy: *Categorizing with catastrophic radii in numerical minimization*, Set-Valued Var. Analysis 29 (2021) 1–28.

[10] A. B. Levy: *Analyzing basins of attraction in numerical minimization*, preprint.

[11] M. Locatelli: *On the multilevel structure of global optimization problems*, Comp. Optim. Appl. 30 (2005) 5–22.

[12] M. A. Luersen, R. Le Riche: *Globalized Nelder–Mead method for engineering optimization*, Computers Structures 82 (2004) 2251–2260.

[13] J. A. Nelder, R. Mead: *A simplex method for function minimization*, Computer J. 7 (1965) 308–313.

[14] B. T. Polyak: *Newton's method and its use in optimization*, Eur. J. Oper. Res. 181 (2007) 1086–1096.

[15] R. T. Rockafellar, R. J.-B. Wets: *Variational Analysis*, Springer, Berlin (1998).

[16] A. Saha & U. Feudel: *Riddled basins of attraction in systems exhibiting extreme events*, Chaos 28 (2018), art.no. 033610.

[17] J. C. Sprott, A. Xiong: *Classifying and quantifying basins of attraction*, Chaos 25 (2015), art. no. 083101.

[18] K. T. Tsang: *Basin of attraction as a measure of robustness of an optimization algorithm*, in: 14$^{\text{th}}$ Int. Conf. Natural Computation, Fuzzy Systems and Knowledge Discovery (ICNC-FSKD), IEEE (2018) 133–137.

[19] M. van Turnhout, F. Bociort: *Instabilities and fractal basins of attraction in optical system optimization*, Optics Express 17 (2009) 314–328.

[20] E. E. Zotos: *Investigating the Newton-Raphson basins of attraction in the restricted three-body problem with modified Newtonian gravity*, J. Appl. Math. Comput. 56 (2018) 53–71.

[21] E. E. Zotos, Md S. Suraj: *Basins of attraction of equilibrium points in the planar circular restricted five-body problem*, Astrophys. Space Sci. 363 (2018), art. no. 20.

[22] E. E. Zotos, Md S. Suraj, A. Mittal, R. Aggarwal: *Comparing the geometry of the basins of attraction, the speed and the efficiency of several numerical methods*, Int. J. Appl. Comput. Math. 4 (2018), art. no. 105, 18p.